Transverse Flux Type Cylindrical Linear Synchronous Motor for Large Thrust Using Generic Armature Cores for Rotary Machinery

Jung-Seob Shin, Takafumi Koseki, and Houng-Joong Kim

***Abstract* -- Linear motors have been of great interest in industries. Especially, the permanent magnet linear synchronous motor (PMLSM) has contributed to its popularization in industrial fields. Among technical performance required to PMLSM, large thrust is an important when considering conveyance of heavy materials such as large glass. The authors propose transverse flux type cylindrical linear synchronous motor for large thrust using generic armature cores for rotary machinery. In this paper, the structure and operational principle of the proposed motor are described. Also, thrust is both theoretically and numerically analyzed by magnetic circuit method and field calculation using the Finite Element Method (FEM).**

***Index Terms*-- Transverse flux type machinery, Cylindrical linear synchronous motor, Large thrust, Flux leakage, Finite element method.**

I. INTRODUCTION

COMPARED with mechanical rotary-translational motion transformation such as ball-skrew drive, direct linear drives have many advantages including low noise, easy maintenance, and high positioning accuracy.

There are many types of linear motors including linear synchronous, linear induction, and linear stepping motors. Especially, the permanent magnet linear synchronous motor (PMLSM) has contributed to the popularization in industrial fields due to the advent of rare earth magnet.

In general, characteristics required to PMLSM in industrial fields are large thrust, high positioning accuracy and simple structure, *etc*. Among these characteristics, large thrust is an important technical performance requirement for PMLSMs. The transverse flux type machinery (TFM) is an ideal alternative [1]-[3]. However, conventional TFM has a relatively complex structure that requires relatively large manufacturing effort [4].

The authors propose transverse flux type cylindrical linear synchronous motor using generic armature cores for rotary machinery.

In this paper, the basic structure and operational principle are explained in Section II. The preliminary design of thrust for simple estimation and a method for reducing cogging force applied in the proposed model are then introduced in Section III. Design and verification of the proposed model through field analysis using the finite element method (FEM) is explained in Section IV. Finally, evaluation on thrust in the three-phase configuration is conducted.

Jung-Seob Shin is with the Department of Electrical Engineering, The University of Tokyo, Tokyo 113-8656, Japan.
(e-mail: jungseobshin1008@koseki.t.u-tokyo.ac.jp)
Takafumi Koseki is with the Department of Electrical Engineering, The University of Tokyo, Tokyo 113-8656, Japan.
(e-mail: takafumikoseki@ieee.org)
Houng-Joong Kim is with KOVERY Co. Ltd, 987-4, Gosaek-dong, Gwonseon-gu, Suwon, Gyeonggi-do, 441-813, Korea (e-mail: ceo@sjroyalmotion.com).

II. TRANSVERSE FLUX TYPE CYLINDRICAL LINEAR SYNCHRONOUS MOTOR

A. The Principle of Generating Thrust

The principle of generating thrust in the proposed model is shown in Fig. 1.

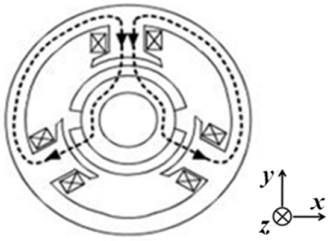

(a) Cross-section of a general rotary synchronous motor

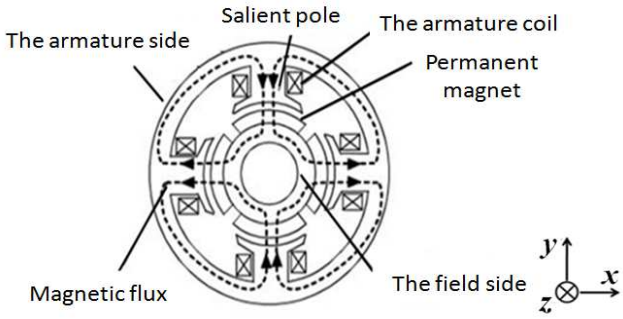

(b) Cross-section of the proposed linear motor

Fig. 1. The principle of generating thrust.

In general rotary synchronous machinery, the number of the armature poles is different from that of the field magnets, as shown in Fig. 1(a). Under this condition, the rotor rotates by applying armature current that has phase differences of 120 degrees to each armature coil.

However, if the number of the armature poles is the same with that of the field magnets as shown in Fig. 1(b), the rotor does not rotate because magnetic balance between the armature and field sides is maintained.

When the armature current is applied to the armature coil in this condition, the moving magnetic field interacts with the field magnets and thus longitudinal force to drive the armature side along *z*-axis is generated.

B. Basic Structure and Operational Principle

Fig. 2 shows the fundamental configuration of the three-phase unit in the proposed model.

In the whole configuration as shown in Fig. 2(a), the armature and field sides are a mover and a stator,

respectively. The armature side consists of three armature units and these units are in non-magnetic material box. The field side consists of field units and these units are in stainless pipe and fixed at both ends.

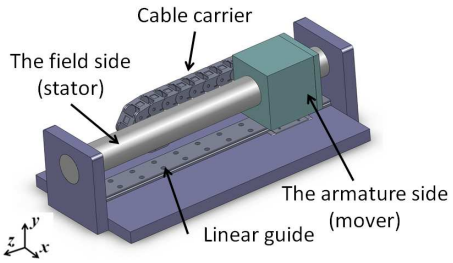

(a) The whole configuration

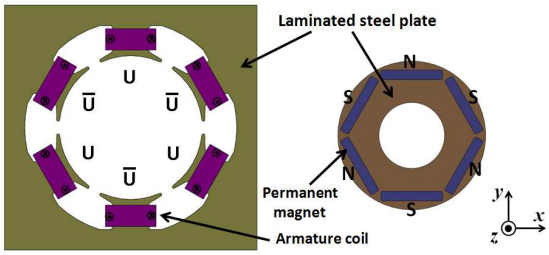

(b) The armature and field unit
(The left side shows an armature unit and the right one shows a field unit.)

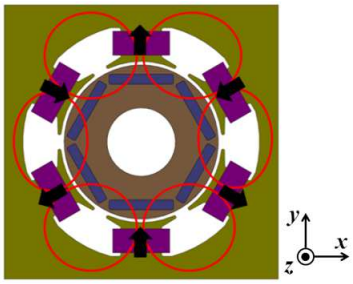

(c) Six balanced magnetic circuits (The red circles denote flux paths.)

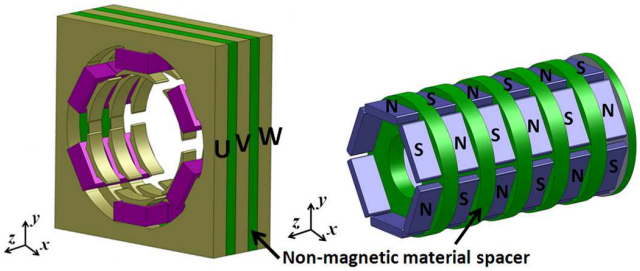

(d) Configuration along moving direction
(Iron cores in the field side are removed for easy understanding.)

Fig. 2. Fundamental configuration of the three-phase unit.

In an armature unit, generic armature cores of brushless DC motor are directly used as iron cores. An armature unit has six salient poles and concentrated windings, as shown in Fig. 2(b). Every armature coils are wound in series with phase differences of 180 degrees. By applying current to these coils, they are excited with electrical phase differences of 180 degrees. In Fig. 2(b), -U is a current component shifted 180 degrees from U.

A field unit consists of six field magnets and iron core, as shown in Fig. 2(b).

Iron cores employed in the armature and field sides can be simply fabricated with laminated steel plates along *z* direction.

When a field unit is accurately located in the center of an armature unit, magnetic circuit is formed, as shown in Fig. 2(c). The flux from the field magnet goes radially through the air gap into a tooth of the armature unit. This transverse flux passes circumferentially along the armature core and finally returns to the field magnet, completing a magnetic circuit. In this manner, the cross-sectional symmetrical magnetic form of six balanced magnetic circuits is created.

In this condition, the normal attractive force between the armature and field sides can be inherently compensated. Even though uncompensated normal force is generated by the unbalance of the air gap, it can be mitigated as internal stress in the armature core in which all armature poles are structurally connected with the same back yoke. For that reason, relatively easy mechanical support and assembly can be achieved.

In fundamental configuration of the three-phase unit, armature cores are arranged along the moving direction *z* with mechanical phase differences of 120 degrees, as shown in Fig. 2(d). The method of winding in each armature core is the same as in Fig. 2(b).

The field magnets polarized radially are arranged along moving direction *z* in an alternate manner. Each row of the field magnet has electrical phase differences of 180 degrees. Between a pair of units, there is a non-magnetic material spacer for magnetic separation between each iron cores. By applying three-phase AC current to each armature coil, the proposed model is exited as a three-phase AC linear synchronous motor.

C. Consideration of Field Magnet Configuration for Large Thrust

Generally, thrust is proportional to the back electromotive force (EMF) and the armature current. When the driving speed is kept constant, the back EMF is determined by the flux linking with the armature coil.

A carefully designed field magnet configuration may realize large back EMF. That is to say, it is possible to increase the rate of the effective flux linking with an armature coil under the condition of fixed amount of the field magnet.

In the initial development stage, the authors proposed two types of field magnet configurations in order to compare their performance on thrust, as shown in Fig. 3. One was magnet configuration defined as Type I in which an armature pole was faced with a field magnet near the air gap and the other was that defined as Type II in which a field magnetic pole was created by adjacent two permanent magnets.

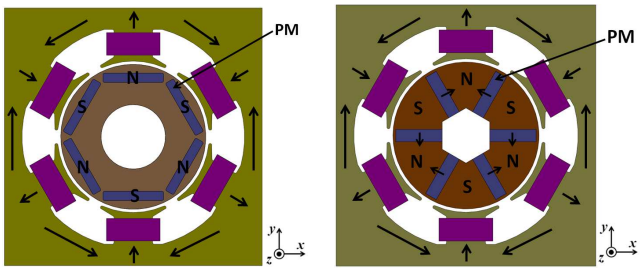

(a) Type I (b) Type II

Fig. 3. The two types of field magnet configurations. (The black arrows denote flux flows.)

The authors expected larger thrust could be obtained in Type II. From the three-dimensional FEM calculations,

however, it was found that no larger thrust could be obtained in spite of our initial expectation [5]. This is due to flux leakage. For that reason, the authors has concluded that the field magnet configuration in Type I is appropriate for a transverse flux type cylindrical PMLSM.

III. Preliminary Design of The Proposed Model

The authors have employed magnetic circuit method in the preliminary design stage and made some assumptions as follows [6]-[7].

(a) The field unit is accurately located in the center of the armature unit.
(b) Permeability of iron cores is infinitely large. Magnetic saturation is neglected.
(c) Slot effect can be taken into account by Carter's factor.
(d) Flux leakage is neglected. All the flux from the field magnet flows into the armature teeth and then link to armature coil.

A. The Air Gap Flux Density

From the above assumptions, a magnetic circuit under no-load condition can be illustrated as Fig. 4.

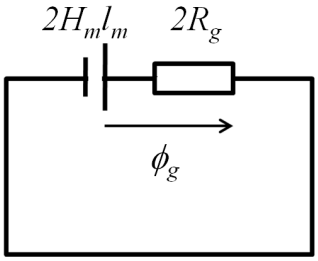

Fig. 4. A magnetic circuit under no-load condition.

A magnetic circuit under no-load condition is based from the flux path denoted in Fig. 2(c). If magnetic reluctance in armature core is neglected, a magnetic circuit can be derived from two magnets and air gap components and can be expressed as

$$H_m l_m + R_g \phi_g = 0 \tag{1}$$

where H_m is the magnetic-field component of magnet, l_m is the magnet length in the magnetization direction, R_g is the magnetic reluctance in the air gap, and ϕ_g is the air gap flux.

From (1), H_m can be expressed as (2). In (2), B_g is the air gap flux density, l_{gc} is the air gap length considered Carter coefficient, and μ_0 is permeability of air.

$$H_m = -\frac{R_g \phi_g}{l_m} = -\frac{B_g l_{gc}}{\mu_0 l_m} \tag{2}$$

The operating flux density on the demagnetization characteristic B_m can be expressed as (3) assuming that it is straight line. B_r is remanence of the field magnet.

$$B_m = B_r + \mu_0 H_m \tag{3}$$

Also, the air gap flux density B_g, the air gap flux ϕ_g, and the magnet flux ϕ_m can be calculated as follows. In (5) and (6), A_m, A_g are the cross-sectional areas of a magnet and the air gap, respectively.

$$B_g = \mu_0 H_g \tag{4}$$

$$\phi_g = B_g \times A_g \tag{5}$$

$$\phi_m = B_m \times A_m \tag{6}$$

By using (1)-(6), the air gap flux density under no-load condition can be expressed as (7).

$$B_g = \frac{B_r}{\left(\frac{A_g}{A_m} + \frac{l_g}{l_m}\right)} \tag{7}$$

If the dimension of the air gap and the air gap length are constant and flux leakage is neglected, the air gap flux under a no-load condition is affected by A_m and l_m.

The effective design for large air gap flux is to select A_m and l_m as large as possible. It means the design for large MMF of the field magnet and relatively small magnetic reluctance, which results in large flux in a magnetic circuit. However, A_m and l_m cannot be infinitely large due to a limited space in the field side, manufacturing cost, and mechanical strength. For that reason, proper selection of A_m and l_m is important in the real design of PMLSM.

If the air gap flux under no-load condition by moving an armature unit is distributed as shown in Fig. 5, it can be expressed by Fourier series. The fundamental component of the air gap flux under no-load condition and its density is (8). In (8), a is a half-length of the field magnet in the moving direction and τ_p is pole pitch. z is the distance in the moving direction and can be expressed by velocity v multiplied by time t.

$$\phi_g(z) = \frac{4\phi_g}{\pi}\sin\left(\frac{\pi a}{2\tau_p}\right)\sin\left(\frac{\pi z}{\tau_p}\right) = \frac{4B_g A_g}{\pi}\sin\left(\frac{\pi a}{2\tau_p}\right)\cos\left(\frac{\pi z}{\tau_p}\right)$$

$$B_g(z) = \frac{\phi_g(z)}{A_g} = \frac{4B_g}{\pi}\sin\left(\frac{\pi a}{2\tau_p}\right)\cos\left(\frac{\pi z}{\tau_p}\right) \tag{8}$$

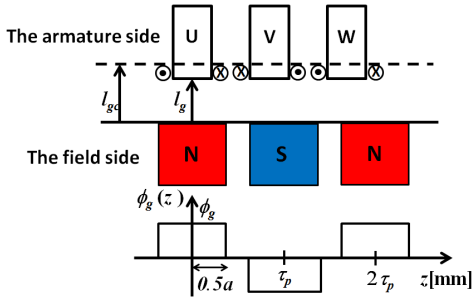

Fig. 5. The air gap flux distribution by moving an armature unit.

B. Thrust

If flux leakage is negligible, all the flux from the field magnets is linked with armature coils and the back electromotive force (EMF) can be expressed as (9). In (9), N is the number of winding turns on a salient pole.

$$E(z) = -N\frac{d\phi_g(z)}{dt} \tag{9}$$

Maximum thrust per an armature unit can be simply estimated by (10). In (10), P_{out} is electromagnetic power, E_{rms} is the RMS value of the back EMF, p is the number of poles in a field unit, and I is armature current.

$$F_{thrust} = p\frac{E_{rms} I}{v} = \frac{\sqrt{2}p\pi B_g A_g N I}{2\tau_p}\sin\left(\frac{\pi a}{2\tau_p}\right) = F_t \sin\left(\frac{\pi a}{2\tau_p}\right) \tag{10}$$

From (10), thrust is generally determined by electrical load *NI* multiplied by magnetic load B_g when other conditions are constant.

C. Cogging Force Reduction

Reduction of cogging force is one of the most important aspects in the design of PMLSM.

The authors have focused on slot-pole combination to reduce cogging force. In the case of rotary synchronous machinery, the higher the least common multiple (LCM) of slot-pole is, the lower the cogging torque can be achieved.

The authors have decided to apply nine core-eight pole combination to the proposed model in the stage of selecting numbers of armature cores and field poles in moving direction [8]. Hence, nine armature cores are faced with eight field magnets in moving direction, as shown in Fig. 6.

In preliminary design stage, the authors decided the total length 108mm of the armature side along the moving direction. Hence, pole pitch τ_p and slot pitch τ_s are 13.5 mm and 12 mm, respectively.

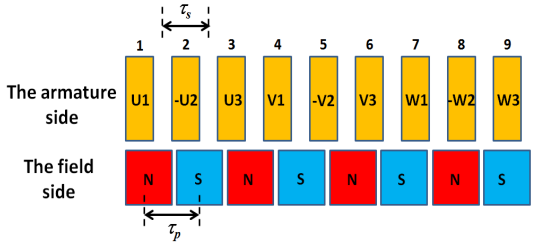

Fig. 6. Nine core-eight pole combination. (-U, -V, and -W are the current components shifted 180 degrees from U, V, and W.)

IV. Design and Verification of The Proposed Model Using FEM

A. Three-dimensional Modeling for Field Analysis

A design employing tools for a numerical field calculation is useful because they provide useful information, including flux leakage, flux distribution, and magnetic saturation, *etc*.

The authors have conducted a field analysis using FEM in order to design the model for case studies and have verified fundamental characteristics. In the field analysis, the JMAG-Designer 10.4.3h, a well-known commercial package, has been used [9]. The three-dimensional mesh model and primary specifications are shown in Fig. 7 and Table I.

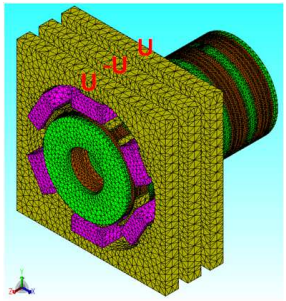

Fig. 7. The three-dimensional mesh model in the FEM calculation.

In field analysis, the authors focused on the armature core width in the moving direction defined as d_a. Geometrically, d_a is inversely proportional to the winding turn per an armature pole due to a decrease of the width of the space $0.5(\tau_s - d_a)$ in which armature coil is wound. It represents the decrease of electrical load by increasing the magnetomotive force (MMF).

Also, three armature cores per a phase were selected for the numerical calculation to avoid unacceptably large computational efforts. In addition, periodic boundary condition was applied to save computation time. The size of the field magnets was properly selected considering spatial limitation and mechanical strength in the field side.

TABLE I
PRIMARY SPECIFICATIONS IN FEM CALCULATION

Item	Quantity
An armature core [mm]	80w × 80h × d_a
A field core [mm]	22.5r × 10d
A magnet [mm]	18.8w × 2.9h × 10d
A non-magnetic material spacer [mm]	80w × 80h × (τ_s-d_a) (The armature side) 22.5r × 3.5d (The field side)
Core-pole combination	9-8
Mechanical air gap length [mm]	1
Pole pitch τ_p [mm]	13.5
Slot pitch τ_s [mm]	12
Velocity *v* [m/s]	1
Armature current *I* [A]	5
Material used as iron core	50JN230 (JFE-steel Corp.)
Permanent magnet	N50M (Shin-Etsu Chemical Co. Ltd.)

B. Effective Flux

All the flux from field magnets does not contribute to generate thrust. That is to say, flux leakage exists. It causes a decrease of the back EMF, which results in a decrease of thrust.

The authors defined the flux that contributes to generate thrust as the effective flux and calculated it from flux linking to armature coil. Fig. 8 shows the result of the effective flux. The maximum effective flux is proportional to d_a due to small magnetic reluctance in the armature core.

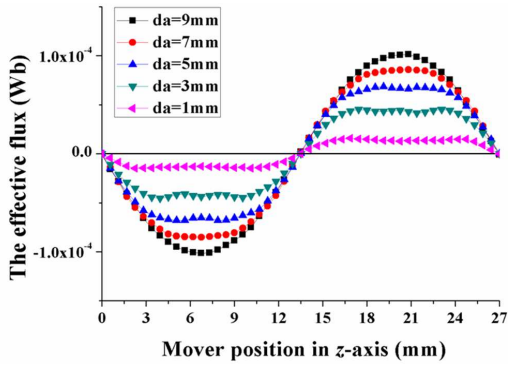

Fig. 8. The numerical result of the effective flux.

From the result in Fig. 8, the authors defined the flux leakage coefficient k_l as expressed in (11). In (11), $\phi_{g\_Theoretical}$ is the maximum value of theoretical air gap flux defined in (8), ϕ_{eff_FEM} is the maximum effective flux.

$$k_l = \frac{\phi_{eff\_FEM}}{\phi_{g\_Theoretical}} \tag{11}$$

C. *Total Longitudinal Force*

Total longitudinal force per a phase acting in moving direction consists of cogging force and thrust.

Here, let us define that maximum thrust per a phase is obtained from difference between total longitudinal force and the cogging force in the mover position where maximum thrust is generated, as written in (12). Cogging force has been calculated by applying virtual displacement principle, as expressed in (13). In (13), W is magnetic energy stored in a phase, which is calculated as consequence of numerical electromagnetic field calculation.

$$F_{t\_1phase} = F_{total\_1phase} - F_{c\_1phase} \tag{12}$$

$$F_{c\_1phase} = -\frac{dW}{dz}\bigg|_{\phi=const.} \tag{13}$$

Fig. 9 and Table II show the numerical results of thrust and cogging force, and the winding turn per an armature pole.

The maximum thrust is at d_a=3 mm. In this point, multiplication of structurally determined winding turn N and effective flux reaches maximum value. Hence, when other variables are fixed, the optimal design for thrust means finding the point where multiplication of electric load and magnetic load reaches maximum value.

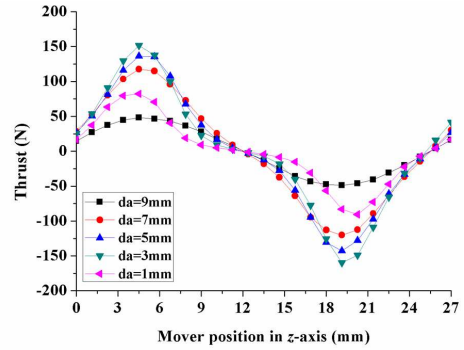

(a) Thrust

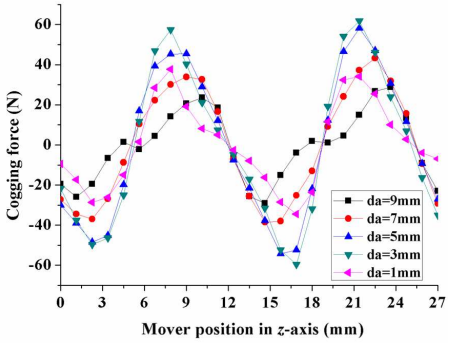

(b) Cogging force

Fig. 9. The numerical result of thrust and cogging force.

TABLE II
WINDING TURN PER AN ARMATURE POLE

The armature core width d_a [mm]	1	3	5	7	9
Winding turn [Turns]	119	91	77	50	21

However, as mentioned in previous section, cogging force is also important aspect in the design of a PMLSM because large cogging force causes force ripple, which results in a poor positioning accuracy. The authors have evaluated this aspect using the ratio of cogging force to thrust. Fig. 10 shows the ratio of cogging force to thrust.

From the result, the authors have decided that d_a=7 mm was the best point in the proposed model. At this point, maximum values of total longitudinal force, cogging force, and thrust are 125.95 N, 38.48 N, and 118.81 N. The FEM value of thrust is 8 % smaller than the theoretical value in Table III, which is nearly the same result when flux leakage coefficient at the point k_l=0.92 is applied.

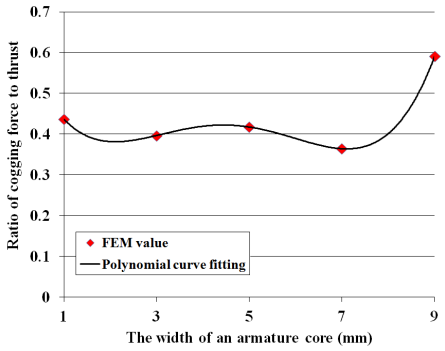

Fig. 10. Ratio of cogging force to thrust.

TABLE III
THEORETICAL RESULTS OF THE PROPOSED MODEL

Item	Quantity
Maximum air gap flux density under no-load condition B_g [T]	0.77
The air gap length considered Carter coefficient l_{gc} [mm]	1.27
Maximum thrust of three cores per a phase F_{thrust} [N]	134.41

V. EVALUATION IN THE THREE-PHASE CONFIGURATION

A. *Total Thrust and Cogging Force per Three-phase*

Total thrust per three-phase has been calculated from the result per a phase, as shown in (14). Maximum thrust in nine core-eight pole combination is 178.21 N.

$$F_{t\_total}(z) = 1.5 \times F_{t\_1phase}(z) \tag{14}$$

The cogging force per three-phase has been calculated by superposing the FEM result per a phase, as shown in (15). In (15), end-effect is assumed to be negligible.

$$F_{d\_total}(z) = F_{d\_1phase}(z) + F_{d\_1phase}\left(z - \frac{2}{3}\tau_p\right) + F_{d\_1phase}\left(z + \frac{2}{3}\tau_p\right) \tag{15}$$

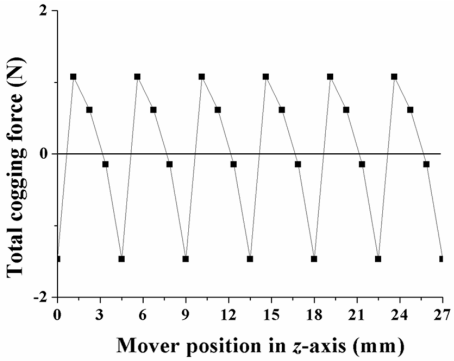

Fig. 11. The cogging force per three-phase.

The numerical result of cogging force per three-phase is

shown in Fig. 11. The maximum value of total cogging force is reduced to about 1.5 N by nine core-eight pole combination and it is about 1% of the thrust.

B. Thrust Density

The authors have calculated thrust density based on the following and compared it with other proposals [10], [11]. Table IV shows thrust density in the proposed model and other commercial products.

In comparison of thrust density, rated thrust has been used. In the case of the proposed model, relatively conservative rated current and thrust have been selected.

(a) The total volume V_t in which the armature side is faced with the field side F_{volume}.
(b) The total dimension S_t in which thrust is generated $F_{dimension}$.
(c) The total weight W_t of mover included in coil mass, non-magnetic material F_{weight}.

TABLE IV
COMPARISON OF THRUST DENSITY

Item	The proposed model	Single-sided type [10]	Double-sided type [10]	Coreless type [10]	Tubular type [12]
Rated thrust [N]	178.21	800	2000	750	780
Rated current [A]	5	11.4	29.7	10.2	8.4
Cooling method	Natural	Heat sink			-
V_t [m^3]	0.69 $\times 10^{-3}$	2.6 $\times 10^{-3}$	8.7 $\times 10^{-3}$	3.7 $\times 10^{-3}$	8.2 $\times 10^{-3}$
S_t [m^2]	15.6 $\times 10^{-3}$	45.0 $\times 10^{-3}$	117.0 $\times 10^{-3}$	102.2 $\times 10^{-3}$	104.5 $\times 10^{-3}$
W_t [kg]	2.962	11.5	43	5	27
F_{volume} [kN/m^3]	257.8	306.5	227.8	200.0	94.5
$F_{dimension}$ [kN/m^2]	11.4	17.7	17.1	7.3	7.5
F_{weight} [N/kg]	60.2	69.6	46.5	150	28.8

VI. CONCLUSION

A transverse flux type cylindrical linear synchronous motor using generic armature cores for rotary machinery has been proposed. The following technical advantages have been discussed.

(a) Large thrust
Large thrust is evaluated by thrust density.
(b) Cogging force reduction
Cogging force is significantly reduced by applying nine core-eight pole combination.
(c) Compatibility with conventional ball-skrew actuators
Structurally similar cylindrical structure is employed.
(d) Structural mitigation of the normal attractive force
It could be mitigated by the cross-sectional symmetrical magnetic form of six balanced magnetic circuits in generic armature cores for rotary machinery
(e) Easy assembly and manufacturing
Iron cores employed in both the armature and field sides could be simply fabricated with laminated steel plates.

In the design, thrust has been both theoretically and numerically analyzed by magnetic circuit method and field calculation using FEM, respectively.

Thrust is proportional to the multiplication of armature magnetomotive force NI and field flux density B_g in the air gap. Based on this fact, this paper has proposed a design method to find the optimal ratio of NI and B_g for maximizing the thrust in a limited space for the proposed transverse flux type cylindrical linear synchronous motor.

VII. REFERENCES

[1] H. Weh, H. Hoffman, and J. Landrath, "New permanent magnet excited synchronous machine with high efficiency at low speeds," in Proc. *Int. Conf. Elect. Mach.*, 1988, pp. 35-40.
[2] J.H. Chang, D.H. Kang, J.Y. Lee, and J.P. Hong, "Development of transverse flux linear motor with permanent magnet excitation for direct drive applications," *IEEE Trans. Magn.*, vol. 41, no. 5, pp. 1936–1939, May 2005.
[3] D. K. Hong, B. C. Woo, D. H. Koo, and D. H. Kang, "Optimum design of transverse flux linear motor for weight reduction and improvement thrust force using response surface methodology," *IEEE Trans. Magn.*, vol. 44,no. 11, pp. 4317-4320, Nov. 2008.
[4] S. D. Joao and V. Mauricio, "Transverse flux machine : what for? ", *IEEE Multidisciplinary Engineering Education Magazine*, Vol. 2,No. 1, pp. 4-6, March 2007.
[5] J. S. Shin, T. Koseki, and H. J. Kim, "The design of flux concentrated type transverse flux cylindrical PMLSM for high thrust", *The International Symposium on Linear Drives for Industry Applications (LDIA2011)*,Netherlands, 2011.
[6] Krishnan Ramu, *Permanent Magnet Synchronous and Brushless DC Motors*, CRC Press/Taylor & Francis, 2009.
[7] Jacek F. Gieras and Zbigniew J. Piech, *Linear synchronous motors: transportation and automation systems*, CRC Press, 1999.
[8] J. Jung, J. Hong, and Y. Kim, "Characteristic Analysis and Comparison of IPMSM for HEV According to Pole and Slot Combination", *IEEE Vehicle Power and Propulsion Conference*, VPPC 2007, pp. 778-783, 2007.
[9] JSOL Corp.
http://www.jmag-international.com/.
[10] Yasukawa Electric Corp.
Available: http://www.yasukawa.co.jp/.
[11] GMC Hillstone Co. Ltd.
Available: http://www. ghc.co.jp/product/shaft.html.

VIII. BIOGRAPHIES

Jung-Seob Shin (M'11) received Master degree of Electrical Engineering from The University of Tokyo, Tokyo, Japan, in 2011, in the laboratory of Prof. T. Koseki. He is currently working toward the Ph.D. degree in Electrical Engineering at The University of Tokyo, Tokyo, Japan. His interests include linear synchronous motor and motor design.

Takafumi Koseki (S'87–M'92) received the Ph.D. degree in electrical engineering from The University of Tokyo, Tokyo, Japan, in 1992. He is currently an Associate Professor with the Department of Electrical Engineering, The University of Tokyo. His current research interests include public transport systems, particularly linear drives, and the analysis and control of traction systems. Dr. Koseki is a member of the Institute of Electrical Engineers of Japan, the Japan Society of Mechanical Engineering, the Japan Society of Applied Electromagnetics and Mechanics, and Verein Deutscher Ingenieure.

Houng-Joong Kim received the Ph.D. degree in electrical engineering from Musashi Institute of Technology, Tokyo, Japan, in 1997. He was with Hitachi Ltd., Japan, until 2007, where he is involved in linear drives research and invented the tunnel actuator as a large thrust and precise-positioning PMLSM. His current research interests include linear drives and motor design. He is currently working as CEO in KOVERY Co. Ltd, Korea.